Oxidation of Pt(111) under Near-Ambient Conditions

D. J. Miller,[1,2] H. Öberg,[3] S. Kaya,[1,2] H. Sanchez Casalongue,[2] D. Friebel,[1,2] T. Anniyev,[1,2] H. Ogasawara,[2] H. Bluhm,[4,5] L. G. M. Pettersson,[3] and A. Nilsson[1,2,3,*]

[1]*Stanford Institute for Materials and Energy Sciences, SLAC National Accelerator Laboratory, 2575 Sand Hill Rd, Menlo Park, California 94025 USA*

[2]*Stanford Synchrotron Radiation Lightsource, SLAC National Accelerator Laboratory, 2575 Sand Hill Rd, Menlo Park, California 94025, USA*

[3]*Department of Physics, AlbaNova University Center, Stockholm University, S-106 91 Stockholm, Sweden*

[4]*Advanced Light Source, Lawrence Berkeley National Lab, Berkeley, California 94720, USA*

[5]*Chemical Science Division, Lawrence Berkeley National Lab, Berkeley, California 94720, USA*

(Received 21 April 2011; published 4 November 2011)

The oxidation of Pt(111) at near-ambient O_2 pressures has been followed *in situ* using x-ray photoelectron spectroscopy (XPS) and *ex situ* using x-ray absorption spectroscopy (XAS). Polarization-dependent XAS signatures at the O K edge reveal significant temperature- and pressure-dependent changes of the Pt-O interaction. Oxide growth commences via a PtO-like surface oxide that coexists with chemisorbed oxygen, while an ultrathin α-PtO_2 trilayer is identified as the precursor to bulk oxidation. These results have important implications for understanding the chemical state of Pt in catalysis.

DOI: 10.1103/PhysRevLett.107.195502 PACS numbers: 81.65.Mq, 68.43.Bc, 68.43.Fg, 82.65.+r

Surface oxides with markedly different activities than the metallic surface can form under the O_2-rich conditions employed in many Pt-based industrial processes [1], including the electrochemical oxygen reduction reaction (ORR) [2], CO oxidation [3–5] and the Ostwald process [6]. However, surface-sensitive techniques that can distinguish different oxidation states, e.g., electron-based spectroscopies, are mostly incompatible with the elevated O_2 pressures ($> 10^{-5}$ Torr) required to oxidize Pt. Consequently, even though (111)-oriented facets are the most abundant close-packed surfaces on the Pt nanoparticles [7] typically employed in industrial catalysis, oxide growth on Pt(111) remains poorly understood.

Exposing Pt(111) to O_2 under ultrahigh vacuum (UHV) conditions yields chemisorbed $p(2 \times 2)$-O domains with an oxygen coverage, θ, at saturation of 0.25 ML [8,9]. However, oxygen phases with $\theta > 0.25$ ML can be prepared in UHV either by using reactive oxygen species, e.g., NO_2 [10–12] and atomic oxygen beams [13,14], or by irradiating saturated O_2 adlayers, e.g., with x rays [15]. In particular, NO_2 yields a network of linear protrusions that was ascribed to a surface-oxide phase with square-planar Pt-O coordination similar to that of bulk PtO [10].

The first *in situ* studies of Pt(111) under high O_2 partial pressures employed surface x-ray diffraction (SXRD) [16]. At near-atmospheric O_2 pressures (> 380 Torr) and above 520 K the formation of O-Pt-O trilayers similar to those found in α-PtO_2 is observed [16]. However, the precursors to the trilayer oxide have not been characterized; in particular, it is unknown whether the PtO-like surface oxide identified in UHV could also form at elevated O_2 pressures, i.e., under conditions approaching those found in heterogeneous catalysis.

Using a photoemission system that can operate at near-ambient pressures ($P < 5$ Torr) [17], we have followed the oxidation of Pt(111) by O_2 by means of x-ray absorption (XAS) and x-ray photoelectron (XPS) spectroscopies. With the aid of density functional theory (DFT) simulations, we demonstrate that oxide growth involves phase transitions from chemisorbed O to two different surface oxides whose structures resemble PtO in the initial stages of oxidation and α-PtO_2 at the onset of bulk oxidation.

The experiments were performed at beam line 11.0.2 of the Advanced Light Source (ALS) using the ambient-pressure XPS end station [17,18]. Oxygen layers were prepared by dosing a Pt(111) crystal (cleaned using standard procedures [8]) with up to 5 Torr O_2. XPS was performed *in situ*, while Auger-yield XAS was measured after evacuating O_2, i.e., under UHV conditions; XPS confirmed that the oxygen layers were stable during spectral acquisition. DFT calculations [19] using the PBE exchange-correlation functional [20] were performed with the GPAW program [21,22], which is a real-space-grid-based all-electron DFT code implemented in the projector augmented-wave [23] (PAW) formalism. XAS spectra were calculated [24] using the half-core-hole transition-potential approach [25], as implemented in GPAW [26].

XPS spectra for O/Pt(111) with coverages up to 2.1 ML are shown in Fig. 1. Surface and bulk Pt atoms of adsorbate-free Pt(111) give rise to Pt $4f_{7/2}$ components at 70.5 and 70.9 eV, respectively [8]. The formation of $p(2 \times 2)$-O domains at 1×10^{-5} Torr O_2 and 300 K yields an additional ''chemisorbed'' Pt $4f_{7/2}$ component at 71.1 eV, an asymmetric O $1s$ structure at 529.7 eV [8,27], and a single XAS peak close to threshold

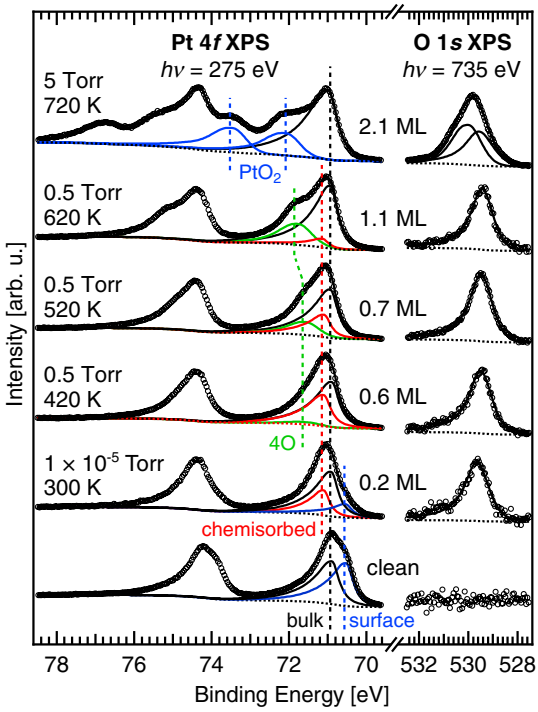

FIG. 1 (color online). Pt 4f (left) and O 1s (right) XPS spectra for O/Pt(111), deconvoluted using asymmetric Voigt and Gaussian-broadened Doniach-Šunjić functions, respectively; a Shirley-type background (dashed line) was removed from all spectra. Excepting $\theta = 2.1$ ML, which was prepared at 5 Torr, 720 K but whose spectrum was acquired at 0.5 Torr, 620 K, the same $P(O_2)$, T conditions were employed for sample preparation and spectral acquisition.

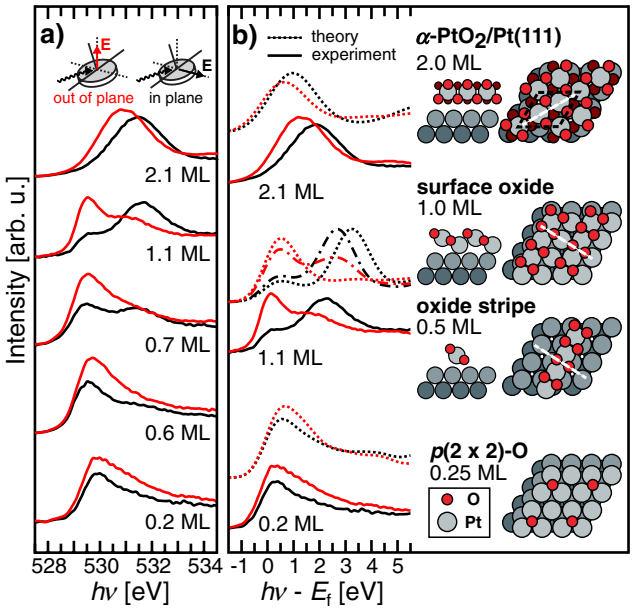

FIG. 2 (color online). Experimental O K-edge XAS spectra (solid lines) are shown in (a) and compared in (b) against simulations (dashed) of the adjacent model structures. Side views of the model structures are cross sections along the dashed lines; the dashed rhombus denotes a (2×2) supercell of the Pt(111) substrate. Results for the 1.0 ML surface oxide and isolated oxide chain are shown using dashed and dashed-dotted lines, respectively. Simulations were obtained by convoluting the GPAW output with a Gaussian of 0.45 eV full-width at half-maximum (fwhm), except for α-PtO_2/Pt(111), for which 0.7 eV was used; these widths were determined from the fwhm of the associated O 1s XPS peaks. Experimental spectra reflect removal of background signal from the Pt substrate and were placed on a B.E. scale in (b) by subtracting the O 1s XPS B.E. All spectra are area normalized ~30 eV above threshold.

(~ 529.9 eV) for both in-plane and out-of-plane polarizations [Fig. 2(a)]. As found in Ref. [8], the out-of-plane spectrum is slightly broader and more intense; otherwise, pronounced polarization dependence is not observed. GPAW simulations [Fig. 2(b)] reproduce all salient features of the observed spectra, thus validating the adopted theoretical approach.

With $P(O_2)$ fixed at 0.5 Torr, the coverage rises steadily from 0.4 ML at $T = 300$ K until saturation (1.1 ML) is attained at ~620 K. Other than the disappearance of the surface peak, below 0.6 ML the only discernible change in Pt 4f XPS is a slight broadening of the chemisorbed component toward high binding energy (B.E.). The corresponding XAS spectra are qualitatively similar in all respects to those obtained at 0.25 ML and, as in previous experimental [10] and theoretical studies [29,30], are best reproduced by chemisorbed structure models in which the O adatoms occupy fcc sites; i.e., our results support the growth of $p(2 \times 1)$-O domains.

An additional Pt 4f feature between 71.6 and 71.7 eV ("4O") grows in above 420 K when $P(O_2) = 0.5$ Torr ($0.6 < \theta < 1.1$ ML). This is accompanied by a ~ -0.2 eV shift of the O 1s XPS peak, which, while smaller than the experimental resolution (~ 0.3 eV), is matched by a comparable shift of the O K-edge absorption threshold, as expected for a system with metallic screening of the core-ionized O$1s^{-1}$ final state. The concomitant observation of strongly polarization-dependent XAS signatures confirms the growth of a chemically distinct new oxygen phase. In particular, we observe an additional high-energy XAS feature that is significantly more pronounced and located $\sim +0.7$ eV (531.6 eV) higher in energy in the in-plane spectrum than in the out-of-plane spectrum.

To address whether the 4O phase could coexist with chemisorbed O, an oxygen layer generated at 0.5 Torr and 570 K ($\theta = 0.8$ ML) was exposed to 2×10^{-8} Torr H_2 [Fig. 3(a)]. Removing up to 0.5 ML of this layer suppressed the near-threshold peak of the in-plane XAS spectrum without significantly affecting the high-energy feature; accordingly, the 4O component of the Pt 4f peak attenuates more rapidly than the chemisorbed component [Figs. 3(a) and 3(c)]. We note, however, that the 4O layers could be removed completely by longer H_2 exposures

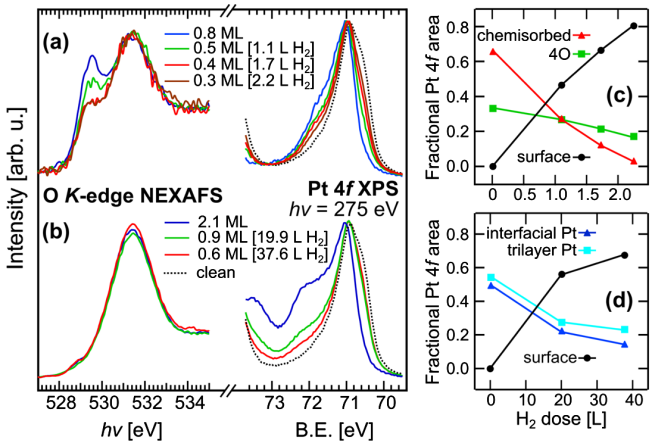

FIG. 3 (color online). In-plane O K-edge XAS spectra (left) and Pt $4f_{7/2}$ XPS spectra (right) obtained after H_2 treatment (2×10^{-8} Torr H_2 at 300 K) of Pt(111) oxidized at (a) 0.5 Torr O_2 and 570 K ($\theta = 0.8$ ML) and (b) 5 Torr O_2 and 720 K ($\theta = 2.1$ ML). XAS spectra are area normalized ~30 eV above threshold. (c) and (d) show the fraction of the total Pt $4f$ peak area associated with each oxygen phase as obtained by deconvoluting the Pt $4f$ XPS spectra in (a) and (b), respectively.

(> 4 L, 1 L = 1×10^{-6} Torr s). Since the high-energy feature exhibits no energy shift and the XAS spectra of the 0.3 ML H_2-treated oxygen layer and a saturated 4O layer (1.1 ML) are in good agreement, H_2-induced structural rearrangements cannot explain the attenuation of the near-threshold peak. The high-energy feature is therefore associated exclusively with the 4O phase, whereas the near-threshold peak can contain an additional chemisorbed contribution. We moreover assign the double-peaked signature of the 0.30 ML H_2-treated layer [Fig. 3(a)] to a nearly pure 4O phase.

The strong polarization dependence of the 4O XAS spectrum indicates a highly anisotropic ligand field of the surface Pt atoms: simulations of high-coverage (i.e., $\theta >$ 0.5 ML) all-fcc chemisorbed structures and high-symmetry subsurface configurations (e.g., O atoms in the tetrahedral hollows located below on-surface hcp sites) fail to reproduce the observed spectra. The 4O phase exhibits O $1s$ and Pt $4f$ core-level shifts [$\Delta_O \sim -0.2$ eV, $\Delta_{Pt} \sim +0.7$–0.8 eV, measured with respect to $p(2 \times 2)$-O (529.7 eV) and bulk Pt (70.9 eV), respectively] highly comparable to those reported for 1D oxide chains with square-planar Pt-O coordination that form at the step edges of Pt(533) [6] ($\Delta_{Pt} \sim +0.55$–0.65 eV) and Pt(332) [4] ($\Delta_O \sim -0.2$ eV, $\Delta_{Pt} = +0.45 \pm 0.07$ eV), indicating that the coordination environment within the 4O phase could be similar. Accordingly, the 4O XAS signature is qualitatively reproduced using the 1 ML surface-oxide model structure depicted in Fig. 2(b), which comprises extended oxide chains with Pt-O bonds oriented almost parallel (~ 15°) to the (111) plane. This structure, proposed by Hawkins *et al.* [30], is generated by occupying selected hcp sites between the close-packed oxygen rows of the $p(2 \times 1)$-O phase and represents the most stable 1 ML configuration identified by those authors using a (2×2) supercell.

However, the 1 ML structure can be relaxed further by using larger supercells. Indeed, a single oxide stripe adsorbed on a $(2\sqrt{3} \times 4)$ supercell of Pt(111) yields improved agreement with the observed 4O spectrum [Fig. 2(b)]: the separation between the near-threshold and high-energy in-plane features (2.2 eV) better matches experiment (2.1 eV), while the high-energy shoulder observed in the out-of-plane direction is now reproduced. Additional simulations (not shown) indicate that the reduced peak separation arises from the longer Pt-O bonds of the isolated stripe ($d = 1.95$, 2.06 Å vs 1.93, 1.96 Å in the original structure): whereas the stripe can adopt a local configuration resembling bulk PtO ($d = 2.04$ Å), bond lengthening in the 1 ML structure incurs a large energy penalty. The high-energy shoulder in the out-of-plane spectrum arises from the increased tilt of the isolated stripe with respect to the (111) plane (~ 29° vs ~15°), which enhances the spectral weight of O $2p$ hybrid orbitals associated with Pt-O σ^* bonds. Although the absence of a superstructure in LEED prevents more detailed structural conclusions, our simulations clearly identify the 4O phase as a surface oxide comprising square-planar PtO_4 units.

Drastic changes in both O $1s$ and Pt $4f$ XPS are observed upon exposure to ~5 Torr O_2 above 720 K ($\theta >$ 1.1 ML): the O $1s$ peak broadens and shifts to higher B.E., while the Pt $4f$ spectrum exhibits—in addition to the bulk peak—two broad, similarly intense features at 72.1 and 73.5 eV. The latter component was also observed after exposing Pt(111) to atomic O [13,14] and *ex situ* following reaction with 750 Torr O_2 at 900 K [31]; given the 74.1 eV B.E. of bulk α-PtO_2, it is assigned to Pt atoms with six O nearest neighbors. As demonstrated below, these highly oxidized Pt atoms reside within α-PtO_2(0001) trilayers. Assuming that the surface is uniformly covered by these trilayers, a simple argument based on the mismatch between the in-plane lattice constants of α-PtO_2 (3.10 Å) and Pt(111) (2.77 Å) leads to an estimate of ~1.3 trilayers when $\theta = 2.1$ ML. However, only a weak (1×1) structure is observed in LEED, suggesting that the PtO_2-like oxide most likely exists as small domains comprising one or two trilayers.

The Pt $4f$ feature at lower B.E. (72.1 eV) is ascribed to Pt atoms at the interface between trilayer and metallic substrate; the smaller Δ_{Pt} arises from both reduced O coordination and more effective metallic screening. The broadened O $1s$ peak indicates that at least two chemically distinct oxygen species are present. We identify two components at 529.7 and 530.1 eV, which on the basis of screening arguments and the binding energies of chemisorbed O (529.7 eV [8]) and bulk α-PtO_2 (530.2 eV [31]) are assigned to O atoms in the lower and upper layers of the

trilayer, respectively. While we are unable to identify XAS features associated with adsorbed OH or H_2O [28], additional measurements, e.g., using vibrational spectroscopy, are required to completely exclude that termination of the oxide surface by such species contributes to the broadening of the O 1*s* XPS feature.

PtO_2-trilayer formation coincides with drastic changes in the polarization dependence of XAS, which indicates large rearrangements of the coordination environment of the surface Pt atoms. Both in-plane and out-of-plane spectra now exhibit a single broad peak centered at 531.5 and 530.8 eV, respectively, which is associated with transitions to unoccupied O 2*p*–Pt 5*d* hybrid states. Partial removal of the trilayer oxide using 2×10^{-8} Torr H_2 did not induce discernible changes in XAS [Fig. 3(b)]; accordingly, the two oxide-derived Pt 4*f* XPS components attenuate at comparable rates upon H_2 exposure [Fig. 3(d)]. Similar behavior was observed for the trilayer oxide that forms on Rh(111) [32] and clearly indicates that a single phase of oxidic Pt is present beyond 1.1 ML. XAS simulations of a single trilayer on Pt(111) are shown in Fig. 2(b). The simulations predict a single peak near threshold that is shifted to higher energy ($\sim +0.4$ eV) in the in-plane spectrum, which agrees well with the observed +0.6 eV shift. We therefore propose that the Pt coordination environment within the surface oxide generated at 2.1 ML resembles the octahedral ligand field of bulk α-PtO_2.

In summary, beyond a critical chemisorbed coverage of $\sim$0.50 ML the oxidation of Pt(111) proceeds via a PtO-like surface-oxide phase, followed by PtO_2-like trilayers that could nucleate at steps or defects [33]. A comparison with oxide growth on other 4*d* and 5*d* Pt-group metals is instructive. Pd(111) also forms a surface oxide, Pd_5O_4, that coexists with chemisorbed O [34], but at oxygen chemical potentials much lower than those required to generate the PtO-like phase. This suggests that there is a greater kinetic hindrance to Pt oxidation, which could be associated with the larger cohesion energy of Pt (-5.84 eV) compared to Pd (-3.89 eV); that PtO-like oxide chains form on the more open (2×1)-Pt(110) surface already at 355 K and $\sim$0.01 Torr supports this interpretation [35,36]. Interestingly, whereas the ultrathin trilayer oxide identified on Pt(111) is preceded by a PtO-like surface oxide, analogous oxidic precursors to the trilayer phases that form on Rh(111) [32,37] and Ir(111) [38] have not been found; the elevated temperatures required to initiate bulk-oxide growth on all three surfaces suggest, however, that the trilayer phase passivates the surface against further oxidation.

The role of the Pt surface oxides identified here in heterogeneous catalysis should be considered when optimizing the size distribution, morphology, alloy composition and core–shell structure of novel catalysts. Indeed, it was recently shown that the electrochemical oxidation of Pt(111) could also proceed via a PtO-like surface oxide [2] that is associated with a significant activation barrier for oxide reduction and that could, in turn, be responsible for the overpotential of Pt-promoted ORR. This result accords with the observation that the square-planar surface oxide reacts much less readily with hydrogen than does chemisorbed oxygen [see Fig. 3(a)]: understanding oxide-related degradation processes could therefore be critical for obtaining efficient and robust catalysts for fuel-cell applications [2,39].

This work is supported by the Department of Energy, Office of Basic Energy Sciences, Division of Materials Sciences and Engineering, under contract DE-AC02-76SF00515, and by the Swedish National Research Council. This research was partly carried out at the Advanced Light Source, an Office of Science User Facility operated for the U. S. Department of Energy Office of Science by Lawrence Berkeley National Laboratory. The DFT calculations were performed on resources provided by the Swedish National Infrastructure for Computing (SNIC) at Center for Scientific and Technical computing LUNARC.

*nilsson@slac.stanford.edu

[1] E. Lundgren *et al.*, J. Phys. Condens. Matter **18**, R481 (2006).
[2] D. Friebel *et al.*, Phys. Chem. Chem. Phys. **13**, 262 (2011).
[3] M. D. Ackermann *et al.*, Phys. Rev. Lett. **95**, 255505 (2005).
[4] J. G. Wang *et al.*, Phys. Rev. Lett. **95**, 256102 (2005).
[5] A. L. Gerrard and J. F. Weaver, J. Chem. Phys. **123**, 224703 (2005).
[6] S. Günther *et al.*, J. Phys. Chem. C **112**, 15 382 (2008).
[7] N. Seriani and F. Mittendorfer, J. Phys. Condens. Matter **20**, 184023 (2008).
[8] C. Puglia *et al.*, Surf. Sci. **342**, 119 (1995).
[9] D. J. Miller *et al.*, J. Chem. Phys. **133**, 224701 (2010).
[10] S. P. Devarajan, J. A. Hinojosa Jr., and J. F. Weaver, Surf. Sci. **602**, 3116 (2008).
[11] R. Getman *et al.*, Phys. Rev. Lett. **102**, 076101 (2009).
[12] D. H. Parker, M. E. Bartram, and B. E. Koel, Surf. Sci. **217**, 489 (1989).
[13] C. R. Parkinson, M. Walker, and C. F. McConville, Surf. Sci. **545**, 19 (2003).
[14] J. F. Weaver, J.-J. Chen, and A. L. Gerrard, Surf. Sci. **592**, 83 (2005).
[15] Y. S. Kim *et al.*, J. Chem. Phys. **133**, 034501 (2010).
[16] C. Ellinger *et al.*, J. Phys. Condens. Matter **20**, 184013 (2008).
[17] D. F. Ogletree *et al.*, Rev. Sci. Instrum. **73**, 3872 (2002).
[18] See supplemental material at http://link.aps.org/supplemental/10.1103/PhysRevLett.107.195502 for additional details regarding the experimental setup and for a description of complementary XAS simulations performed using the FEFF8.4 code.
[19] Chemisorbed (oxide) slabs comprise four (five) atomic layers of Pt(111), two of them fully relaxed, separated by

14 Å (15 Å) of vacuum and supporting O on one side, see Ref. [9]. ($\sqrt{3} \times 2$) surface cells were used for all slabs except the oxide stripe, for which a ($2\sqrt{3} \times 4$) cell was used. For α-PtO_2/Pt(111), we assumed coincidence between ($\sqrt{3} \times \sqrt{3}$)$R30°$ and (2×2) cells of the α-PtO_2(0001) trilayer and Pt(111), respectively. This structure was optimized using computed spectra rather than the total energy, since the neglect of van der Waals forces causes uncertainty in the vertical displacement, d_z, of the Pt atoms in the trilayer from the topmost substrate layer. Varying d_z from 2.9 to 4.1 Å while keeping Pt-O distances within the trilayer fixed yielded an optimal d_z of 3.5 Å.

[20] J. P. Perdew, K. Burke, and M. Ernzerhof, Phys. Rev. Lett. **77**, 3865 (1996).

[21] J. Enkovaara *et al.*, J. Phys. Condens. Matter **22**, 253202 (2010).

[22] J. J. Mortensen, L. B. Hansen, and K. W. Jacobsen, Phys. Rev. B **71**, 035109 (2005).

[23] P. E. Blöchl, Phys. Rev. B **50**, 17953 (1994).

[24] PAW setups containing a half-core-hole at the excited O were employed. The XAS cross section was obtained using the Haydock recursion scheme [R. Haydock *et al.*, J. Phys. C **5**, 2845 (1972)] with 2000 Lanczos vectors to avoid explicitly constructing the unoccupied states. The periodic boundary conditions necessitated large supercells ($15 \times 15 \times 30$ Å^3) to eliminate core-hole interactions between adjacent cells.

[25] L. Triguero, L. G. M. Pettersson, and H. Ågren, Phys. Rev. B **58**, 8097 (1998).

[26] M. P. Ljungberg, J. J. Mortensen, and L. G. M. Pettersson, J. Electron Spectrosc. Relat. Phenom. **184**, 427 (2011).

[27] The high-binding-energy tail of the O 1*s* feature arises from shake-up excitations rather than from OH and H_2O species, which desorb from metallic Pt well below 300 K [8,28].

[28] T. Schiros *et al.*, J. Phys. Chem. C **111**, 15 003 (2007).

[29] R. B. Getman, Y. Xu, and W. F. Schneider, J. Phys. Chem. C **112**, 9559 (2008).

[30] J. M. Hawkins, J. F. Weaver, and A. Asthagiri, Phys. Rev. B **79**, 125434 (2009).

[31] M. Peuckert and H. P. Bonzel, Surf. Sci. **145**, 239 (1984).

[32] J. Klikovits *et al.*, J. Phys. Chem. B **110**, 9966 (2006).

[33] S. A. Krasnikov *et al.*, Nanotechnology **21**, 335301 (2010).

[34] E. Lundgren *et al.*, Phys. Rev. Lett. **88** 246103 (2002).

[35] W. X. Li *et al.*, Phys. Rev. Lett. **93**, 146104 (2004).

[36] S. Helveg *et al.*, Surf. Sci. **430**, L533 (1999).

[37] J. Gustafson *et al.*, Phys. Rev. Lett. **92**, 126102 (2004).

[38] Y. B. He *et al.*, J. Phys. Chem. C **112**, 11 946 (2008).

[39] D. Friebel *et al.*, Angew. Chem., Int. Ed. **50**, 10 190 (2011).